11A.5 A COMPARISON OF HIGH-RESOLUTION MESOSCALE FORECASTS USING MM5 AND WRF-ARW

Aijun Deng*, David R. Stauffer and Glenn K. Hunter
Penn State University, University Park, PA

1. INTRODUCTION

The Weather Research and Forecast (WRF) model is a new state-of-the-science mesoscale model framework under development for many years by UCAR and NCEP, and specifically designed for the 1-10 km grid length scales. The advanced research WRF (WRF-ARW) uses more advanced, higher-order spatial and temporal finite differencing schemes than MM5 and also contains cloud-scale 3D sub-grid turbulence closures in addition to many of the model physics packages (e.g., planetary boundary layer (PBL), moist microsphysics, land-surface, convective parameterization) available with MM5. As WRF matures to include more of the important options from MM5 (e.g., data assimilation), it is becoming more attractive for fine-resolution numerical weather prediction (NWP) due to its mass conservation, improved numerics and expanding physics. To help determine the potential added value of transitioning from MM5 to WRF, a direct comparison between MM5 and WRF are presented in this study.

Model simulations during the February 2006 Torino Winter Olympics in northern Italy are used in this current evaluation. Penn State and the Defense Threat Reduction Agency (DTRA) used their on-demand MM5 realtime systems to support hazard prediction and consequence assessment over the complex terrain of the Alps and the Torino plains during the Winter Olympics (Stauffer et al. 2007a). Four nested grids of 36-km, 12-km, 4-km and 1.3-km resolutions were used to produce 24-h forecasts over all the Olympics venues. After the games, six cases representing the great variety of weather scenarios during the 16-day period were chosen for a retrospective comparison study between MM5 and WRF-ARW (Stauffer et al. 2006) and to determine the sensitivity of the meteorological forecast accuracy and HPAC/SCIPUFF predictions to model resolution and four-dimensional data assimilation (Stauffer et al. 2007b).

The WRF runs produced shortly after the games using WRF-ARW 2.1 and presented at last year's workshop (Stauffer et al. 2006), produced some lateral boundary noise problems and missed some important precipitation over the Olympics venues for some of the cases, as compared to the MM5 runs. Nonetheless, statistical differences between these two models without FDDA over the special Italian mesonet data network were relatively small, and suggest that there was no clear statistical advantage of one model over the other for wind, temperature and moisture.

MM5 and WRF subjective and statistical results using the latest WRF version, WRF-ARW 2.2, are compared here with special attention paid to the previous version WRF problems with lateral boundary noise and underprediction of precipitation over the Olympics venues. Section 2 provides the model descriptions, and Section 3 outlines the experimental design. Model intercomparison results are presented in Section 4 with summary and conclusions appearing in Section 5.

2. MODEL DESCRIPTIONS

This study uses the Pennsylvania State University/National Center for Atmospheric Research (PSU/NCAR) mesoscale model, known as MM5, and the advanced research version of the Weather Research and Forecast (WRF-ARW) model.

2.1 MM5 Model

The MM5 is a nonhydrostatic, fully compressible three dimensional primitive equation model with a terrain following sigma (non-dimensional pressure) vertical coordinate (Dudhia 1993, Grell et al. 1995), and Arakawa-B horizontal grid staggering. The MM5 uses a split semi-implicit temporal integration scheme and contains prognostic equations for the three wind components, temperature and water-vapor mixing ratio. In MM5, resolved-scale moist processes are represented using explicit prognostic equations for cloud water or ice and rain water or snow according to a formulation described by Dudhia (1989). The ground temperature is predicted based on a surface energy budget (Slab Force-Restore method) which includes the effects of atmospheric radiation and the surface fluxes which vary based on specified land-use information and soil moisture (Grell et al. 1995).

*Corresponding author address:
Dr. Aijun Deng, 405 Walker Building, University Park, PA 16802, deng@meteo.psu.edu

2.2 WRF-ARW Model

The WRF-ARW is also a nonhydrostatic, fully compressible three dimensional primitive equation model with a terrain-following hydrostatic pressure vertical coordinate (Skamarock et al. 2005, Laprise 1992), denoted by η and defined as

$$\eta = \frac{p_{dh} - p_{dht}}{\mu_d} \quad (1)$$

where $\mu_d = p_{dhs} - p_{dht}$, represents the mass of the dry air in the column, p_{dh} represents the hydrostatic pressure of the dry atmosphere at a given η level, and p_{dht} is the hydrostatic pressure at the top of the dry atmosphere. Like MM5, the prognostic equation for each variable (wind, potential temperature, moisture and hydrometeor fields) uses a flux form.

For temporal discretization, the WRF-ARW solver uses a third-order Runge-Kutta (RK3) time integration scheme, while the high-frequency acoustic modes are integrated over smaller time steps to maintain numerical stability (Wicker and Skamarock 2002). For spatial discretization, ARW solver uses Arakawa-C horizontal grid staggering (Arakawa and Lamb 1977). In the vertical direction, variables are defined identical to that in MM5, with wind/mass fields on half η layers and the vertical velocity and TKE at the full layers.

There are a number of formulations for turbulent mixing and filtering available in the WRF-ARW solver. Some of them are used for numerical reasons, and other filters are meant to represent physical sub-grid turbulence processes. Unlike MM5, the ARW allows sub-grid scale turbulence to be parameterized as it is treated in cloud-scale models - including horizontal mixing. However, when a PBL scheme is used, all other cloud-scale vertical mixing is disabled, and vertical mixing is parameterized in the chosen PBL scheme. Like MM5, WRF-ARW has a variety of physics options for microphysics, cumulus parameterization, PBL physics and atmospheric radiation. For microphysics, this research uses the Single-Moment 3-class (WSM3) scheme (Hong et al. 1998, 2004, and Skamarock et al. 2005).

3. EXPERIMENTAL DESIGN

In order to make a fair comparison, both MM5 and WRF use the exact same grid configuration (i.e. 36/12/4/1.33 km), same initial and lateral boundary conditions, and similar physics (Table 1). No four dimensional data assimilation (FDDA) is used in either MM5 or WRF. Kain-Fritsch cumulus parameterization scheme (Kain and Fritsch 1990) is applied on both 36- and 12-km grids. Both models use simple ice microphysics. Since a new version of WRF v2.2 was released in December of 2006 which allows use of a new WRF Preprocessing System (WPS), the six Olympics cases were rerun using the new WRF-ARW 2.2 with the exact same initial and boundary conditions as used previously. Instead of using WRF Standard Initialization (SI), WPS is used for preprocessing.

Table 1 MM5 and WRF Experimental Design

	PBL Physics	CPS	Radiation	Microphysics	FDDA
MM5	Eta M-Y TKE	KF on 36/12	Dudhia/RRTM	Simple ice	no
WRF	M-Y-J TKE	KF on 36/12	Dudhia/RRTM	WSM-3	no

The domain configuration for both MM5 and WRF is shown in Fig. 1. All domains are 100 x 100

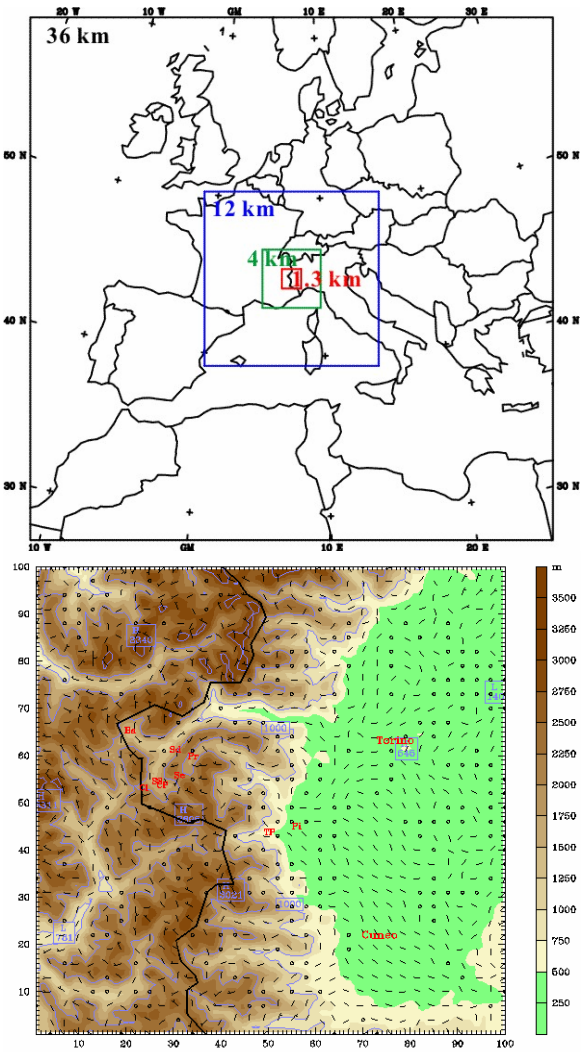

Figure 1. MM5 and WRF four-domain configuration for 2006 Winter Olympics cases (top), and 1.33-km model terrain with Olympics venues (bottom). The domains are centered on the area directly around the Winter Olympics venues in both the complex terrain of the Alps and the flat plains around Torino, Italy.

Table 2. Descriptions of the six case days used for this study.

2006 Torino Olympics Cases		
Case 1	00 UTC, 13 Feb - 00 UTC, 14 Feb	Dry
Case 2	12 UTC, 17 Feb– 12 UTC, 18 Feb	Precip/Wind in Mountains
Case 3	00 UTC, 18 Feb– 00 UTC, 19 Feb	Precip in Mountains
Case 4	12 UTC, 19 Feb– 12 UTC, 20 Feb	Precip in Mountains and on Plains
Case 5	00 UTC, 22 Feb– 00 UTC, 23 Feb	Precip on Plains
Case 6	12 UTC, 25 Feb– 12 UTC, 26 Feb	Light Precip in Mountains and on Plains

grid cells, and all nested domains share a common center in the region of the Winter Olympics in northern Italy. The domains are configured such that the innermost 1.33-km domain is comprised of about half complex terrain (the Alps) and half flat terrain (Torino plains). The six cases chosen for further examination represent the range of meteorological conditions experienced during the course of the Winter Olympics games. Details of the meteorological conditions and the dates of the six cases are given in Table 2.

4. MODEL RESULTS

Three types of model evaluations are provided to analyze the performance of WRF-ARW compared to MM5. First, a statistical analysis is performed to provide an objective measure of model performance. Second, model simulations are run using two separate nesting techniques to further investigate the WRF lateral boundary noise problem that was known to exist in previous experiments with WRF-ARW 2.1. Third, a comparison is made between MM5 simulations of the six Olympics cases and corresponding results using WRF-ARW 2.2.

4.1 Statistical Evaluation

To compare the performance of MM5 and WRF during the period of the Winter Olympics, a statistical

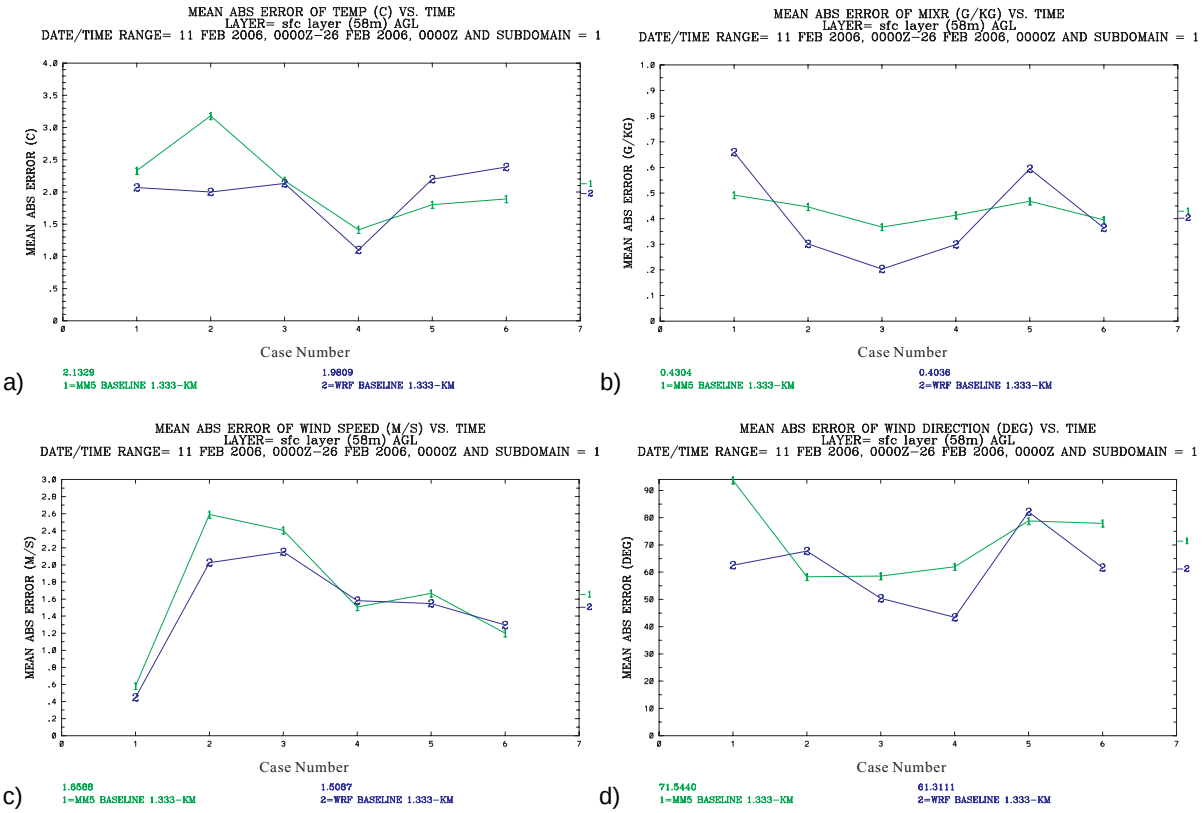

Figure 2. Mean absolute error of a) surface temperature (°C), b) surface water vapor mixing ratio, (g kg $^{-1}$) c) surface wind speed (m s^{-1}), d) surface wind direction (degrees), for the MM5 and WRF 1.33-km model domains, averaged over the 24-h forecast periods for all six cases. Case-averaged values are plotted on right side of figure with numerical values in the experiment key.

evaluation is performed using special mesonet observations within the 1.33-km domain of each model. In this study, statistical averages are computed for the six select cases. The following series of statistical plots shows surface layer time series of mean absolute error (MAE) representing a 24-h average for each of the six cases, as well as an overall average MAE of all six cases. In addition to statistical time series, vertical profiles of MAE are also shown. These profiles represent the six-case average MAE for each vertical level in the two models, and the vertically-averaged MAE. Results from both WRF-ARW 2.1 and WRF-ARW2.2 are statistically similar (not shown), with WRF-ARW 2.2 having a very slight advantage. For nearly all analyzed variables and vertical levels, the statistical averages were slightly smaller for WRF-ARW 2.2. A statistical comparison of MM5 and WRF-ARW 2.2 reveals that despite the amount of improvements that have been made to WRF-ARW, it does not yet demonstrate a clear statistical advantage over MM5 for this series of model simulations. Figure 2 shows surface time series plots of MM5 and WRF MAE for temperature (°C), mixing ratio (g kg^{-1}), wind speed (m s^{-1}) and wind direction (degrees).

The MAE time series comparisons reveal that over the period of the six Winter Olympics cases, neither MM5 nor WRF-ARW has a clear statistical advantage since the differences are quite small. In all time series, WRF-ARW has slightly smaller statistical errors than MM5 when averaged over all six cases, but the significance of the improvement has not been tested. In each of the time series, statistical performance is dependent upon the individual case. For example, in Fig. 2c, MM5 has lower MAE than WRF-ARW for wind speed in two cases (Case 4 and Case 6). In Fig. 2d, however, MM5 has lower MAE than WRF-ARW for wind direction in two different cases (Case 2 and Case 5). The wind direction errors in Fig. 2d tend to be larger for those cases with weaker wind speeds (Stauffer et al. 2007). The statistical results are very similar between the two models against the special observations that are located well within the 1.33-km domain boundaries (Stauffer et al. 2006).

Similar results can be seen in the vertical profiles of MAE in Fig. 3. The model that has the lower statistical scores than the other often flip flops, depending on the vertical level. Much like the time series plots, the WRF-ARW has a slight numerical statistical advantage, but only performs better than the MM5 at all levels for water vapor mixing ratio (Fig. 3b). (The better WRF performance in mixing ratio is particularly interesting since the WRF model appears to have a disadvantage in the precipitation forecasts presented in the following sections.) When averaged over all six cases, however, the error advantage is still less than 0.10 g kg^{-1}

4.2 WRF-ARW Nesting Configuration

Although the statistical results show that WRF may have a slight advantage, other issues were uncovered that would not be clearly distinguishable by a statistical analysis. One critical problem with the WRF-ARW simulations is a band of unrealistic spikes in precipitation fields on nested domains when using the ndown (nestdown) component of the WRF system. That is, the nestdown procedure is used to interpolate the coarser mesh results to the finer grid mesh when using a one-way interactive grid nesting strategy. This is a systematic problem that occurs in all six Olympics cases. As a test, WRF is run using a one-way nesting strategy with al. l four model domains in the same job submission (i.e. the nested lateral boundaries are updated every time step rather than hourly and there is no feedback to the coarser "mother" domains). Figure 4 shows the Case 6, 24-h WRF-ARW forecast without the use of ndown on the 1.33-km domain. Figure 5 shows the same WRF-ARW forecast simulation, where the only difference is that the finer domains are created by ndown steps using 1-hourly output from the mother domain. The results using one-way nesting in a single job without the ndown procedure do not show the same unrealistic spikes in precipitation around the lateral boundaries as that using ndown.

Observations for this case indicate light precipitation in the mountainous terrain and on the plains (not shown). In Fig. 4 (no ndown steps), light precipitation is forecasted to be present in the 12 hours prior to the valid time, with maximum amounts ranging from 8 to 10 mm. In Fig. 5 (with ndown steps), however, unrealistic spikes in precipitation are evident around the lateral boundaries, especially on the northern and western boundaries. Maximum 12-h precipitation forecasts in this simulation are in excess of 150 mm, compared to the 8-10 mm forecasts in the other WRF-ARW simulation.

The noise around the lateral boundaries in WRF-ARW is almost certainly related to an inconsistency between the domains when the nested terrain is not blended with the parent's terrain near the boundaries. The MM5 one-way nestdown results, however, do not show this problem. This issue has been sent to wrf-help, and it is currently under investigation by NCAR.

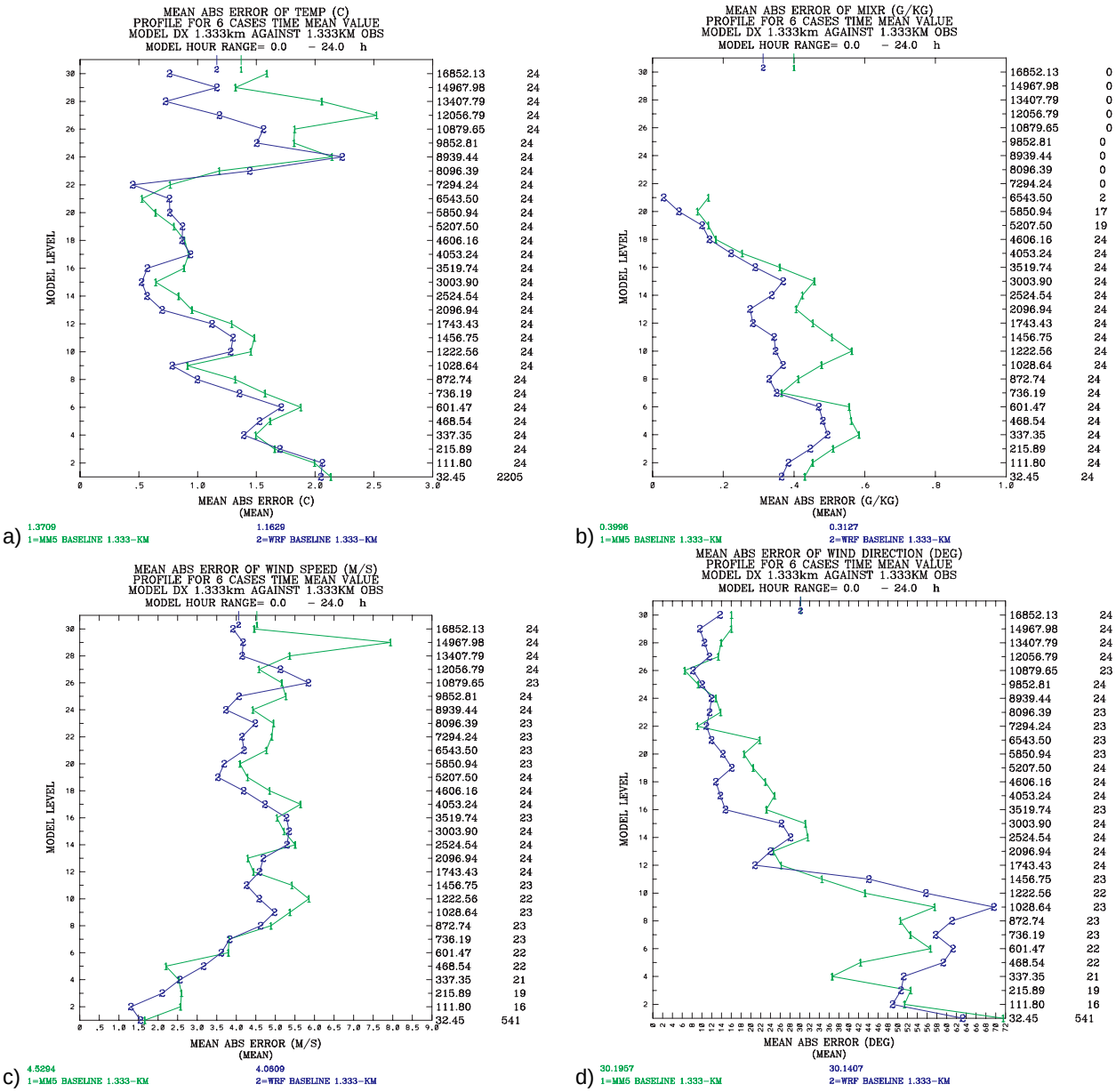

Figure 3. Profile of mean absolute error of a) temperature (°C), b) water vapor mixing ratio, (g kg $^{-1}$) c) wind speed (m s^{-1}), d) wind direction (degrees), for the 24-h forecast period for MM5 and WRF averaged over all six case days on the 1.33-km domain. Vertical averages are plotted at top of figure with numerical values given in the experiment key.

4.3 MM5 vs. WRF-ARW Subjective Results

Based on the statistical analysis in Section 4.1 and the sensitivity of the results to different nesting configurations in Section 4.2, a full subjective analysis of the MM5 and WRF-ARW results for all six cases is performed. The subjective analysis presented here compares one of the six cases from the Winter Olympics (Case 2) that received appreciable amounts of precipitation over the Olympic venues in the mountains during the course of the 24-h simulation.

Case 2, which occurred from 12 UTC, 17 February 2006 to 12 UTC, 18 February 2006, was a case where several observation sites located at Olympics venues reported between 5 cm and 9 cm of snowfall in the 24 -h period (not shown). As each of these observations were recorded at mountain Olympics venues, it is important that the mesoscale models accurately predict precipitation, because of its implications surrounding the games themselves as well as traveling spectators.

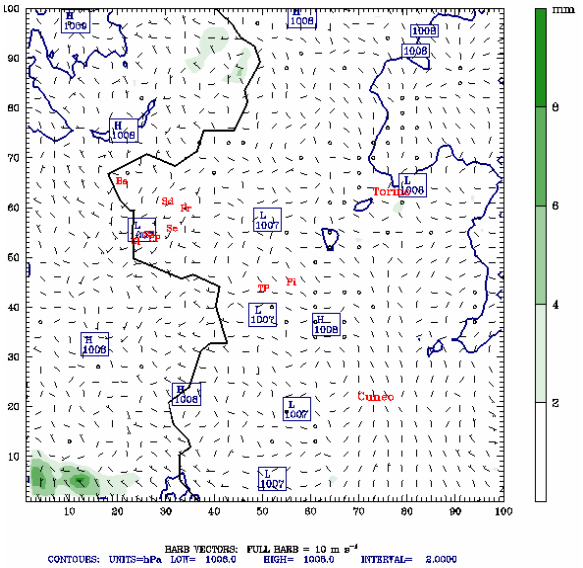

Figure 4. WRF-ARW 24-h 1.33-km resolution 12-h precipitation forecast for Case 6, valid 1200 UTC, 26 Feb 2006. The lateral boundary conditions for this 1.33-km domain were created in the same model job submission as the other domains with no feedback, i.e. ndown was not used.

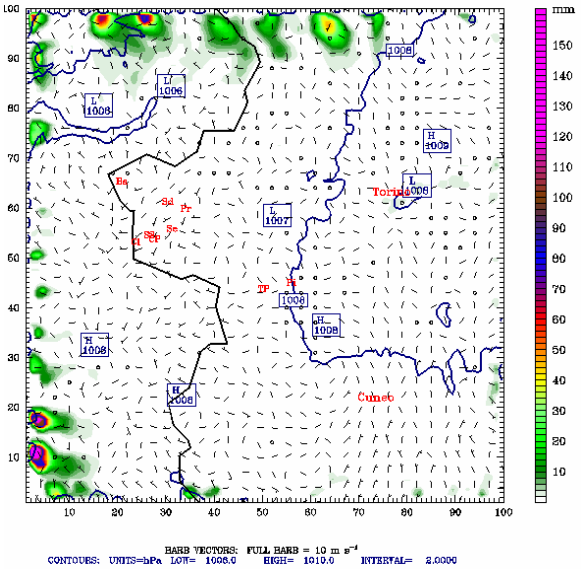

Figure 5. WRF-ARW 24-h 1.33-km resolution 12-h precipitation forecast for Case 6, valid 1200 UTC, 26 Feb 2006. The lateral boundary conditions for this 1.33-km domain were created using the ndown, with one-way nesting tendencies provided on the fine mesh lateral boundaries based on hourly coarser mesh output.

Predicted 24-h precipitation amounts on the 1.33-km domain are shown for MM5 in Fig. 6, and for WRF-ARW in Fig. 7. A few differences are immediately noticeable between the figures. The MM5 simulated precipitation is more widespread across the mountainous terrain, with slightly lower

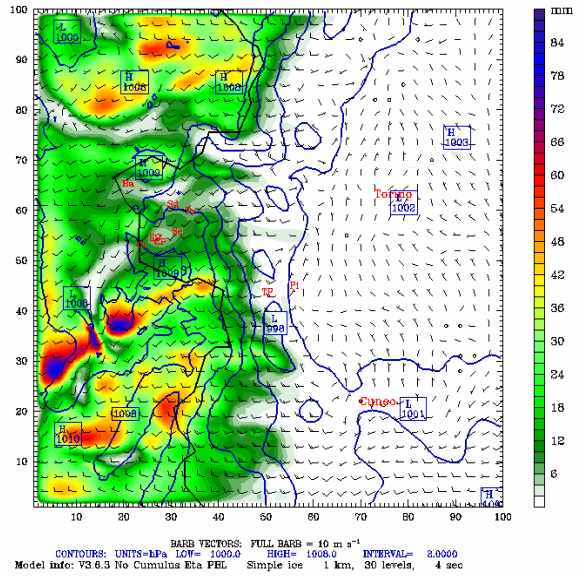

Figure 6. Forecasted 24-h precipitation accumulations (mm) from MM5 on the 1.33-km domain. Precipitation amounts are color-filled according to the scale to right of the plot.

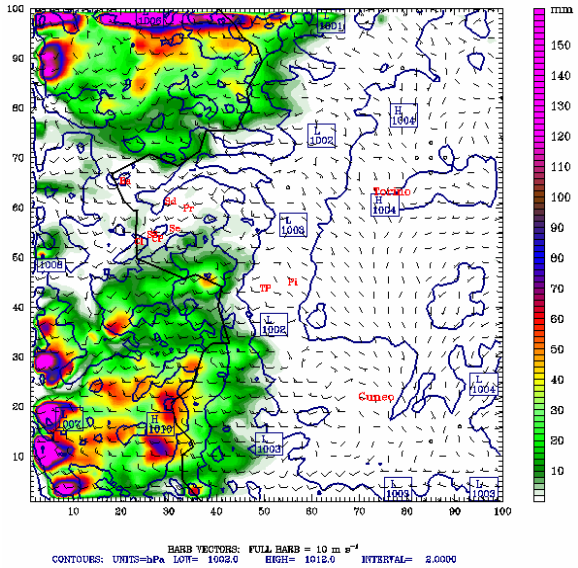

Figure 7. Forecasted 24-h precipitation accumulations (mm) from WRF-ARW on the 1.33-km domain. Precipitation amounts are color-filled according to the scale to right of the plot.

precipitation accumulations near the cluster of Olympics venues (identified by red labels on the precipitation plots). The WRF-ARW simulation has generally heavier precipitation amounts than MM5 in the northern third and southern third of the mountainous terrain area. In the central third area directly surrounding the Olympics venues, however, WRF-ARW is predicting very light, if any precipitation. Observed precipitation amounts in this area were 5 cm of snow (approximately 5 mm of liquid equivalent, assuming a standard 10:1 snow to

water ratio) in Cesana Pariol (CP), 6 cm of snow in Cesana-San Sicario (SS), and 9 cm of snow in Bardonecchia (Ba).

The forecasted precipitation amounts are under-predicted in the WRF-ARW simulation, based on the observed precipitation amounts. The most unfortunate aspect of the under-prediction of precipitation in WRF-ARW is that it happens to be in a location where it was very crucial to this particular modeling application. It can be said, however, that both MM5 and WRF-ARW correctly predicted no precipitation at the locations on the Torino plains, where no precipitation was observed.

It should be noted that Fig. 7 also shows the same unrealistic spikes in precipitation amounts along the lateral boundaries, as discussed in the previous section. During the same period where MM5 predicts slightly greater than 84 mm of liquid precipitation, WRF-ARW predicts amounts greater than 150 mm, nearly double the MM5 prediction. This phenomenon is also apparent in the other four cases that are not discussed or shown here.

In general for all six Olympics cases, WRF-ARW tended to produce smaller area coverage of precipitation within the 1.33-km domain area than MM5. Perhaps this may be related in some way to the enhanced vertical motion fields and numerical noise around the WRF lateral boundaries when using one-way nesting and ndown..

5. CONCLUSIONS

This study shows that the statistical differences between these two models without FDDA were relatively small based on the special surface mesonet data, and the available upper air data, and suggest that while WRF-ARW had slightly smaller errors when averaged over the six Olympics cases, there was no clear advantage of one model over the other for this study. The statistics were computed over the special observation locations apparently far enough from the lateral boundaries where the WRF simulations showed considerable noise.

Results from WRF-ARW have, however, shown some issues that need to be addressed, such as: 1) unrealistic spikes in the precipitation field near the lateral boundaries when the model is one-way nested using ndown steps; 2) missed or under-predicted precipitation in the mountainous Olympics venues region where observations and MM5 predictions showed precipitation; and 3) the tendency for WRF-ARW to produce smaller area coverage for precipitation over the 1.33-km domain area compared to MM5 using similar model physics options, which may possibly be related to the WRF lateral boundary noise problem. Note that these WRF noise problems were only found in these specific conditions: complex terrain, one way nests running in separate job steps, use of ndown and one-hourly lateral boundary condition updates.

6. ACKNOWLEDGMENTS

We acknowledge ARPA Piemonte and Massimo Milelli for providing us their their special mesonet data for the Olympics. Patrick Hayes of NGC/DTRA assisted in a lot of the preparations for the Olympics modeling using MM5, and Laurie Carson of NCAR managed the observation exchange site with the Italians. This work was supported by DTRA through contract DTRA01-03-D-0013 with L-3 Titan.

7. REFERENCES

Arakawa, A. and V.R. Lamb, 1977: Computational design of the basic dynamical process of the UCLA general circulation model. *Methods in Comp. Physics*, **17,** 173-265.

Deng, A., and D.R. Stauffer, 2006: On improving 4-km mesoscale model simulations. *J. Appl. Meteor.*, 45, 361-381.

Dudhia, J., 1989: Numerical study of convection observed during the winter monsoon experiment using a mesoscale two-dimensional model. *J. Atmos. Sci.*, **46**, 3077–3107.

Dudhia, J., 1993: A nonhydrostatic version of the Penn State/NCAR mesoscale model: Validation tests and simulation of an Atlantic cyclone and cold front. *Mon. Wea. Rev.*, **121,** 1493-1513.

Grell, G., J. Dudhia and D.R. Stauffer, 1995: A description of the fifth-generation Penn State/ NCAR mesoscale model (MM5). NCAR Tech. Note NCAR/TN-398+STR, 122 pp.

Hong, S.-Y., H.-M. H. Juang, and Q. Zhao, 1998: Implementation of prognostic cloud scheme for a regional spectral model, *Mon. Wea. Rev*., **126**, 2621–2639.

Hong, S.-Y., J. Dudhia, and S.-H. Chen, 2004: A Revised approach to ice microphysical processes for the bulk parameterization of clouds and precipitation, *Mon. Wea. Rev*., **132**, 103–120.

Kain, J. S. and J. M. Fritsch, 1990: A one-dimensional entraining/detraining plume model and its application in convective parameterization. *J. Atmos. Sci.*, **47**, 2784–2802.

Klemp, J.B., W.C. Skamarock and O. Fuhrer, 2003: Numerical consistency of metric terms in terrain-following coordinates. *Mon. Wea. Rev*. 131, 1229–1239.

Laprise, R., 1992: The Euler equations of motion with hydrostatic pressure as an independent variable. *Mon. Wea. Rev*., **120**, 197-207.

Skamarock, W. J. B. Klemp, J. Dudhia, D. O. Gill, D. M. Barker, W. Wang and J. G. Powers, 2005: A description of the Advanced Research WRF Version2. NCAR Tech. Note NCAR/TN-68+STR, 88 pp. [Available from NCAR Mesoscale and Microscale Meteorology Division, Boulder, CO 80397.

Stauffer, D.R., G.K. Hunter, A. Deng, Y.C. Kwon, P. Hayes, J. Trigg, Jr., 2006: Penn State-DTRA high resolution meteorological modeling for the Torino Winter Olympics, WRF Users' Workshop, Boulder CO, June 21, 4 pp.

Stauffer, D.R., G.K. Hunter, A. Deng, J.T. McQueen, P. Hayes, C. Kiley, 2007a: On the role of atmospheric data assimilation and model resolution on meteorological accuracy and atmospheric transport and dispersion, Preprints, Chemical Biological Information Systems Conference & Exhibition, Austin, TX, Jan 8-12, 6 pp.

Stauffer, D.R., G.K. Hunter, A. Deng, J.R. Zielonka, K. Tinklepaugh, P. Hayes and C. Kiley, 2007b: On the role of atmospheric data assimilation and model resolution on model forecast accuracy for the Torino Winter Olympics, 22nd Conference on Weather Analysis and Forecasting/18th Conference on Numerical Weather Prediction, June 25-29, Park City, UT.

Wicker, L.J., and W.C. Skamarock, 2002: Time-Splitting Methods for Elastic Models Using Forward Time Schemes. *Mon. Wea. Rev.*, **130**, 2088–209.